Michigan State University

National Superconducting Cyclotron Laboratory

FULLY MICROSCOPIC MODEL ANALYSES OF THE ELASTIC SCATTERING OF 200 MeV PROTONS FROM TARGETS OF DIVERSE MASS

P.J. DORTMANS, K. AMOS, and S. KARATAGLIDIS

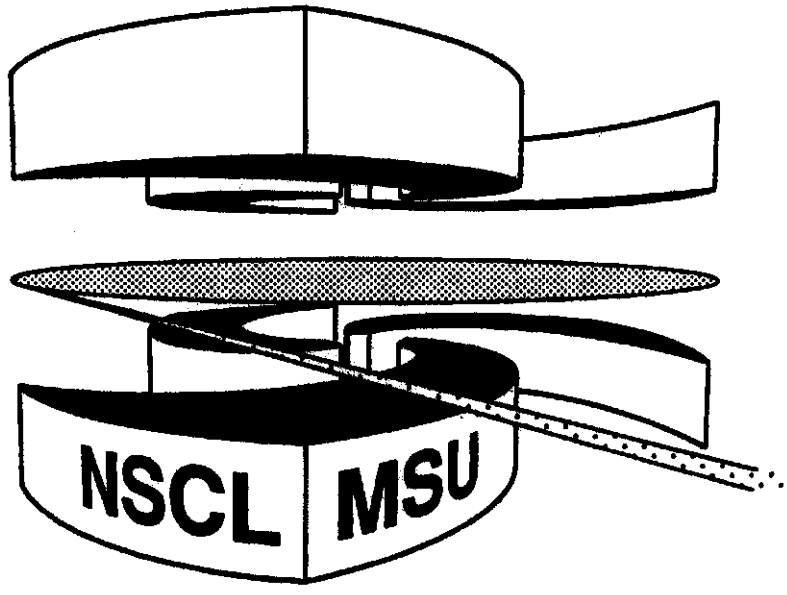

MSUCL-1051

NOVEMBER 1996

Fully microscopic model analyses of the elastic scattering of 200 MeV protons from targets of diverse mass

P. J. Dortmans and K. Amos

School of Physics, University of Melbourne,

Parkville 3052, Victoria, Australia.

S. Karataglidis

National *Superconducting Cyclotron Laboratory,* Michigan *State* University,

East* Lansing, *MI, 48824-1 321

Abstract

Nonlocal optical potentials for the scattering of 200 MeV protons from 22 nuclei, ranging in mass from ^{6}Li to ^{208}Pb, have been defined by folding a complex, medium dependent effective interaction with density matrix elements of each target. The effective interaction is based upon solutions of the Lippmann–Schwinger and Brueckner–Bethe–Goldstone equations having the Paris potential as input. The bound state single particle **wave functions that specify the nuclear density matrices are Woo&-Saxon functions for $A \leq 12$ and harmonic oscillator functions thereafter. The resulting differential cross sections, analysing powers and spin rotations all compare well with the known** data.

I. INTRODUCTION

In recent publications [1,2], the specification and results of a fully microscopic, coordinate space, model analysis of 200 MeV proton scattering from ^{12}C were reported. This energy lies in a 'transition' region between low and intermediate energies in which one expects effects of nonlocalities in the effective nucleon-nucleus *(NA)* interaction, as well as of medium dependent effects in the nucleon-nucleon (NN) effective interaction upon which that *NA* interaction is built, will be important [3,4]. When these are taken into account, excellent fits can be found to the elastic scattering cross sections and analysing powers [1,4]. With appropriate structure input, this was also the case with a number of inelastic scattering cross-section and analysing power data sets and over a range of proton energies [1,5]. The optical potentials for the elastic scattering, and for both the incident and emergent channels in distorted wave approximation (DWA) analyses of the inelastic scattering events, were formed by folding a complex effective interaction with nuclear density matrices. The resulting optical potentials are nonlocal and usually approximated by an equivalent local form. We have chosen to retain the full nonlocal result which then has been used in finding

solutions of (nonlocal) Schrödinger equations to give (elastic) scattering phase shifts and the distorted wave functions needed in DWA calculations. The same effective interaction was taken as the transition operator in the DWA calculations of the inelastic scatterings to many states in ^{12}C. The effective interaction is a mixture of central, two–body spin–orbit and tensor force attributes, with each having a set of four Yukawa functions with complex coefficients. With the interaction in this form, we can use the programme DWBA91 [6] not only to solve the nonlocal Schrödinger equations but also to make fully antisymmetrized, DWA calculations of inelastic scattering events. The ranges and coefficients of the Yukawa functions were defined by accurately mapping the double Bessel transforms of that effective interaction to an appropriate set of infinite nuclear matter g matrices [7]. Those g matrices were obtained from solutions of the Bethe–Brueckner–Goldstone equations [8] in which the starting potential was the Paris NN interaction [9]. We note in passing that there is little sensitivity to the choice of starting interaction. For each nucleus, the nuclear matter density profile required [10–12] was folded with the g matrices. Details of the techniques involved are given elsewhere [1,7]. Given that the NN g matrices are most easily specified in momentum space and the effective interaction form is an approximation, it is sensible to seek to analyse NA elastic scattering with a momentum space solution of the Schrödinger equation. Attempts have been made [12,13], but only recently have such studies used credible g matrices as input [14]. These results [14] reflect reasonable agreement with the data and confirm the need for inclusion of medium effects for low and intermediate energy NA scattering [1,5]. As yet there has not been any sophisticated attempt to analyse inelastic scattering data with a theory defined fully in momentum space and so we maintain interest in using effective interactions and coordinate space models of scattering.

A feature in our process of analysis was that all details required to make the calculations were preset. The effective interaction was defined from a nucleon–nucleon interaction. In the case of ^{12}C [1], the nuclear structure information was taken from complete $(0+2)\hbar\omega$ shell model calculations with the single nucleon wave functions set by fits to elastic electron scattering form factors. Thus the results for both the elastic and inelastic scatterings of

200 MeV protons from ^{12}C were obtained from single calculations. No adjustments (core polarisations) were needed and most proton excitation data were well fit. Similarly, data from the scattering of 200 MeV protons from ^{16}O and of 160 MeV protons from ^{14}N were also well fit [15] when allowance is made for inadequacies in the structure used. Thus the fully microscopic (coordinate space) model for 200 MeV proton scattering is established for a set of $0p$–shell nuclei and it is the purpose of this article to show that to be the case over the entire mass range. For masses $A > 20$, we have not insisted that the single particle (SP) wave functions be set by fits to electron scattering data as we do not have sophisticated shell model wave functions for these.

We consider herein only the elastic scattering channel but take the spin rotation, Q, into account along with the cross sections, $d\sigma/d\Omega$ and analysing powers, A_y. Specifically we have considered 22 targets, namely the $0p$–shell set of ^{6,7}Li, ^{9}Be, ^{10}B, ^{12,13}C, and ^{16}O, the $(1s0d)$–shell set of ^{20}Ne, ^{27}Al, and ^{28}Si, the $0f_{7/2}$–shell set of ^{40,42,44,48}Ca, the pair of ^{56}Fe and ^{58}Ni in mass 50 region, the pair of ^{88}Sr and ^{90}Zr in mass 90 region, the pair of ^{115}In and ^{120}Sn in mass 120 region, and the heavy nuclei, ^{197}Au and ^{208}Pb. Since 200 MeV data was not available for all the nuclei listed above, some 185 MeV data were considered and in the analyses of those, we have used the 200 MeV effective interaction in the folding process along with the appropriate 185 MeV kinematics to give the nonlocal optical model potentials.

II. RESULTS AND DISCUSSION

The results of our calculations of the elastic scattering of 200 MeV protons (185 MeV in select cases) are shown in Figs. 1–11 wherein for each target, the $d\sigma/d\Omega$, A_y and Q from the scatterings are shown in the top, middle and bottom segments respectively. The target is identified in each diagram.

Proton elastic scattering data from the $0p$-shell nuclei [1,15] usually is not sensitive to the choice of either the $0\hbar\omega$ or the $(0+2)\hbar\omega$ shell model space, when using the Cohen and

Kurath [16] and MK3W interactions [17], respectively. However, the elastic electron form factors, especially if transverse form factors exist, can be sensitive to such choices [1,15]. Hence, for completeness, we have set the bound state SP wave functions from fits to the elastic electron scattering data within the $(0+2)\hbar\omega$ shell model space. Where the SP wave functions were determined from fits to proton scattering data, a $0\hbar\omega$ shell model space was employed. We have used the MK3W interaction [17] for the $0p$-shell nuclei, the Brown and Wildenthal interaction [18] for the $1s0d$–shell nuclei, and the FPMI3 [19] for the $0f1p$–shell nuclei. A simple packing model specification whereby the nucleons were placed in the nuclear shells of maximal single particle binding, was used to obtain the shell occupancies for all of the heavier nuclei.

Traditionally one chooses either Woods–Saxon (WS) or harmonic oscillator (HO) functions for the bound state SP wave functions. As was seen previously [1,15], the choice of SP wave functions has some effect on both $d\sigma/d\Omega$ and A_y for elastic proton scattering off of light nuclei. As the atomic mass increases, the distinctions between the results found using the two forms decrease. Therefore we have chosen WS wave functions for nuclei up to (and including) ^{12}C, and HO functions thereafter. The WS bound state potential parameters (listed in Table I) and the oscillator lengths (Table II) for nuclei up to ^{20}Ne were set by matching to the elastic (longitudinal) electron scattering form factors [20]. With the heavy nuclei, we allowed the oscillator lengths to vary slightly from the conventional $A^{(1/6)}$ variation [21] to find the best fit to the proton cross–section data. However the values of the oscillator lengths found for all nuclei do not vary greatly from those defined for the root mean square (r.m.s.) charge radii [11]. The values of those charge radii are listed in Table II [22]. The calculated r.m.s. charge radius are all smaller than those determined from electron scattering analyses [1,15,20]. But it should be noted that for $A \leq 20$ our structures have given very good fits to the elastic electron scattering form factors.

In Fig. 1, the data [23] from the scattering of 200 MeV protons from ^{6,7}Li are compared with the results of our calculations. For these and the other non zero spin $0p$–shell nuclei, contributions from all multipoles have been included, with the non zero components

evaluated in a *DWA*. Such contributions are necessary to achieve the quality of fit to the data [23]. For both nuclei, the cross section and analysing power data are well fit, while no such data are as yet available for comparison with the spin rotation.

In Fig. 2, the ^{9}Be and ^{10}B calculations are shown in comparison with the available data [24]. Again no spin rotation measurements have been reported. In these cases the cross sections are very well reproduced. The analysing powers are also in reasonable agreement with our results, especially as we note the marked effect higher multipole ($J > 0$) contributions have at the larger scattering angles. Their destructive interference is particularly important above 30°.

Even better results, as far as agreement with observation is concerned, are found in the next two figures with the ^{12,13}C measurements [25,26] and our results displayed in Fig. 3 and those from ^{16}O and ^{20}Ne are given in Fig. 4. The data of the latter were taken from Refs. [26,27]. Note that, with the exception of ^{12}C, the *SP* wave functions were taken to be *HO*, fitted to the elastic electron form factors. Spin rotations have been measured from both ^{12}C and ^{16}O and the results of our calculations compare very well with those data. The analysing powers are even better fit (to about 40°) while the cross sections to 60° are extremely well reproduced. There is no data available from ^{20}Ne at or near 200 MeV, but the results of calculations are shown as a prediction. As a large basis projected Hartree–Fock model has been reported for ^{20}Ne [28], data from that as a target (elastic and the inelastic channels) would be of particular interest for analysis.

The scattering data [29,30] from the $1s0d$–shell nuclei, ^{27}Al and ^{28}Si, are shown next in Fig. 5 wherein, as no 200 MeV data was available for ^{27}Al, Uppsala data taken at 183 MeV is shown. For these and all subsequent nuclei, the *SP* wave functions were determined by fits to the proton cross–section data. The measured cross sections and analysing powers are very well fit and through the third peak of the analysing power from ^{28}Si. With increasing mass, the spin dependent variables have more structure. That is also the case with the 200 MeV data [26,27,31] taken from the Ca isotopes. The results are displayed in Figs. 6 and 7. In Fig. 6 the ^{40,42}Ca data and our analyses are presented, while Fig. 7 contains the

^{44,48}Ca data and results. The fits to the cross–section data remain excellent to 60° for all four isotopes as are those to the spin dependent data (to at least 40°). The spin rotation is well fit for both ^{40,48}Ca. For ^{40}Ca, the results compare very favourably with those obtained through a purely momentum space scheme [14].

There are no spin rotation data for scattering from the mass 50 nuclei considered next in Fig. 8, nor are there for the ensuing cases of mass 90 and 120 that are shown in Figs. 9 and 10 respectively. Cross–section and analysing power data have been reported in Refs. [29,32], [33], and [29,34] respectively and the quality of the fits to those given by our calculated results remains very good. Here, the experimental data for ^{56}Fe, ^{90}Zr and ^{115}In were taken at 183 MeV. The ^{56}Fe analysing power result is not as good but the trend with respect to the data is still correct.

Finally the heavy mass targets, ^{197}Au and ^{208}Pb, are considered and the results of our calculations are compared with the data [29,35] in Fig. 11. The results for the 183 MeV ^{197}Au data are not as good as most of the other cases studied, but some slight variation caused either by shell effects or by the data being measured at an energy other than 200 MeV might be anticipated in this case. On the other hand the ^{208}Pb results are very good and of the same level of accuracy as achieved in recent momentum space calculations [14]. The cross–section data are reproduced through the third peak ($\sim 30°$) as are the analysing power and, especially, the spin rotation. We do note, however, that our cross–section results for the scattering from ^{208}Pb are not as good as those found with an earlier microscopic model study [4] wherein, for a number of energies, cross–section shapes over some 11 orders of magnitude were very well reproduced. Yet, we do as well, and perhaps a little better, in reproducing the observed analysing power data. However, our result is that from a single calculation and we have neither optimised the density profile of ^{208}Pb nor adjusted component elements of the NN effective interaction to seek better fits to the data. It is important to note that the interaction used by the previous study [4], was formed similarly to ours, and is energy and medium dependent. Such attributes must be treated in any realistic analysis of medium energy proton scattering from nuclei.

Details of the SP wave functions are given in the Tables with the WS parameters and the orbit binding energies for the five lightest masses considered shown in Table I. As required there is a steady increase with mass in the binding of the $0s$ and $0p$ orbits. We have arbitrarily set the binding energy of the weakly bound orbits at 0.5 MeV. The harmonic oscillator lengths are given in Table II from which it is obvious that the progressive increase of 'b' with mass is not monotonic. This is more evident in the last figure, Fig. 12, wherein the product $bA^{-1/6}$ is shown as a function of $A^{1/3}$. The (heavy mass) expectation that oscillator energies should vary as $41.47A^{-1/3}$ transcribes to the straight line of value 1 in this figure. Most values for masses $A \geq 27$ lie within a few percent of that expectation, but they do tend to be smaller. The exceptions to this are ^{56}Fe and ^{197}Au, the (185 MeV) data sets which were not as well represented as the other nuclei shown. Finally the breakdown of the 'rule' for oscillator energies and lengths when one considers low masses is very evident. In fact for masses to ^{20}Ne, these oscillator lengths vary rather as $(1.35 \pm 0.05)A^{1/12}$.

III. CONCLUSIONS

With no adjustment for light nuclei (A $\leq$ 20) or small variations otherwise of any factor in a fully microscopic model calculation of the elastic scatterings of 200 MeV protons from 22 targets ranging from ^{6}Li through ^{208}Pb, we have found excellent reproduction of the measured differential cross sections usually (over 5 orders of magnitude) and very good to excellent fits to the spin dependent measurables, the analysing powers and spin rotations. The calculations were made using the fully antisymmetrised formalism contained in the programme DWBA91 with effective interactions that involve central, tensor and two–body spin–orbit forces. Those effective interactions were specified by mapping their double Bessel transforms to the NN g matrices of infinite nuclear matter (fermi momenta to 1.5 fm^{-1}) built from the Paris two nucleon potential.

In each case, optical potentials were formed by folding the effective interactions with a specification of each target's single nucleon shell occupancies and appropriate SP wave

functions. Those optical potentials are nonlocal and the scattering phase shifts from which predictions of the measured quantities were specified were obtained by solution of the relevant nonlocal Schrödinger equations. In general, cross–section, analysing power and spin rotation data (where defined) were well fit. Therefore, one can expect to obtain good fits to elastic proton scattering data at intermediate energies with nonlocal optical potentials which are determined from folding realistic effective interactions with the appropriate density profiles.

Use of these optical potentials and of the effective two nucleon interaction as the transition operator in the DWA are being made to investigate inelastic scattering data sets that have been taken with a number of these targets.

ACKNOWLEDGMENTS

This research was supported by by a research grant from the Australian Research Council. Support was also provided by NSF Grant No. PHY94-03666 (MSU).

REFERENCES

[1] S. Karataglidis, P. J. Dortmans, K. Amos, and R. de Swiniarski, Phys. Rev. C **52**, 861 (1995).

[2] S. Karataglidis, P. J. Dortmans, K. Amos, and R. de Swiniarski, Aust. J. Phys. **49** 644 (1996).

[3] L. Ray, Phys. Rev. C **41**, 2816 (1990); J. J. Kelly and S. J. Wallace, Phys. Rev. C **49**, 1315 (1994).

[4] H. V. von Geramb and K. Nakano, in *The Interaction Between Medium Energy Nucleons and Nuclei*, AIP Conf. Proc. 97, edited by H. O. Meyer (AIP, New York, 1982), p. 44; L. Rikus, K. Nakano, and H. V. von Geramb, Nucl. Phys. **A414**, 413 (1984).

[5] P. J. Dortmans, S. Karataglidis, K. Amos, and R. de Swiniarski, Phys. Rev. C **52**, 3224 (1995).

[6] J. Raynal, computer code DWBA (NEA1209/02).

[7] P. J. Dortmans and K. Amos, Phys. Rev. C **49**, 1309 (1994).

[8] M. I. Haftel and F. Tabakin, Nucl. Phys. **A158**, 1 (1970); P. J. Dortmans and K. Amos, J. Phys. **G17**, 901 (1991).

[9] M. Lacombe, B. Loiseau, J. M. Richard, R. Vinh Mau, J. Côté, P. Pirès, and R. de Tourreil, Phys. Rev. C **21**, 861 (1980).

[10] L. R. B. Elton, in *Nuclear Sizes*, Oxford University Press (1961) p. 31; G. R. Satchler, Nucl. Phys. **A579**, 241 (1994).

[11] C. W. De Jager, H. De Vries, and C. De Vries, Atomic Data and Nuclear Data Tables **14**, 479 (1974); H. De Vries, C. W. De Jager, and C. De Vries, *ibid.* **36**, 495 (1987).

[12] T. Mefford, R. H. Landau, L. Berge, and K. Amos, Phys. Rev. C **50**, 1648 (1994).

[13] Ch. Elster and P. C. Tandy, Phys. Rev. C **40**, 881 (1989); Ch. Elster, T. Cheon, E. F. Redish, and P. C. Tandy, Phys. Rev. C **41**, 814 (1990); H. F. Arellano, F. A. Brieva, and W. G. Love, Phys. Rev. C **41**, 2188 (1990); *ibid.* C **42** 1782 (1990); *ibid.* C **43**, 2734 (1991); and references cited therein.

[14] H. F. Arellano, F. A. Brieva, and W. G. Love, Phys. Rev. C **52**, 301 (1995).

[15] S. Karataglidis, P. J. Dortmans, K. Amos, and R. de Swiniarski, Phys. Rev. C **53**, 838 (1996).

[16] S. Cohen and D. Kurath, Nucl. Phys. **73**, 1 (1965).

[17] E. K. Warburton and D. J. Millener, Phys. Rev C **39**, 1120 (1989).

[18] B. A. Brown and B. H. Wildenthal, Ann. Rev. Nucl. Part. Sci. **38**, 29 (1988).

[19] W. A. Richter, M. G. van der Merwe, R. E. Jules, and B. A. Brown, Nucl. Phys. **A523**, 325 (1991).

[20] M. C. Munro, Ph. D. thesis, University of Melbourne, 1994 (unpublished).

[21] B. Hahn, D. G. Ravenhall, and R. Hofstadter, Phys. Rev. **101**, 1131 (1956); R. R. Roy and B. P. Nigam, in *Nuclear Physics*, J Wiley and Sons, 1967, p. 233.

[22] J. M. Delbrouck-Habaru and Daniel M. Dubois, Comp. Phys. Comm. **8**, 396 (1974).

[23] C. W. Glover *et al.*, Phys. Rev. C **41**, 2487 (1990) and J. R. Comfort, private communication; C. W. Glover *et al.*, Phys. Rev. C **43**, 1664 (1991) and J. J. Kelly, private communication.

[24] C. W. Glover *et al.*, IUCF Scientific and Technical Report 1982, p.7; H. Baghaei *et al.*, Phys. Rev. Letts. **69**, 2054 (1992) and J. J. Kelly, private communication.

[25] J. R. Comfort, G. L. Moake, C. C. Foster, P. Schwandt, and W. G. Love, Phys. Rev. C **26** 1800 (1982) and P. Schwandt, private communication; H. O. Meyer, P. Schwandt,

G. L. Moake, and P. P. Singh, Phys. Rev. C **23**, 616 (1981).

[26] E. J. Stephenson *et al.*, IUCF Scientific and Technical Report 1984, p.1.

[27] H. Seifert *et al.*, Phys. Rev. C **47**, 1615 (1993); J. J. Kelly, private communication.

[28] W. C. Ford, R. C. Bailey, and J. Bar-Touv, Phys. Rev. C **4**, 2099 (1971); S. Karataglidis, P. Halse, and K. Amos, Phys. Rev. C **51**, 2494 (1995).

[29] A. Ingemarsson and G. Tibell, Physica Scripta **4**, 235 (1971).

[30] K. H. Hicks *et al.*, Phys. Rev. C **38**, 229 (1988); J. Lui *et al.*, IUCF Scientific and Technical Report 1992, p.11.

[31] P. H. Karen, Ph. D. thesis, University of Virginia, 1993 (unpublished) and J. J. Kelly, private communication; A. E. Feldman *et al.*, Phys. Rev. C **49**, 2068 (1994) and J. J. Kelly, private communication.

[32] J. Lisantti, private communication.

[33] J. J. Kelly *et al.*, Phys. Rev. C **47**, 2146 (1993) and J. J. Kelly, private communication; E. Hagberg, A. Ingemarsson, and B. Sundqvist, Physica Scripta **3**, 245 (1971).

[34] H. Sakaguchi *et al.*, RCNP Annual Report 1993, p.4.

[35] D. A. Hutcheon *et al.* in *Polarization phenomena in Nuclear Physics, 1980* (ed. G. G. Olsen, R. E. Brown, N. Jarmie, W. W. McNaughton, and G. M. Hale) (AIP, New York, 1981) and P. Schwandt, private communication; N. Ottenstein, S. J. Wallace, and J. A. Tjon, Phys. Rev. C **38**, 2272 (1988).

TABLES

TABLE I. Binding energies (in MeV) for SP wave functions determined for WS parameters [22] of $r_o = 1.35$ fm., $a_o = 0.65$ fm., $r_c = 1.05$ fm., and $\lambda = 7.0$.

Orbital	^{6}Li	^{7}Li	^{9}Be	^{10}B	^{12}C
$0s_{\frac{1}{2}}$	−23.93	−25.97	−33.03	−37.17	−38.75
$0p_{\frac{3}{2}}$	−6.45	−8.77	−17.28	−19.78	−22.37
$0p_{\frac{1}{2}}$	−4.44	−6.84	−15.21	−17.81	−20.65
$0d_{\frac{5}{2}}$	−0.50	−0.50	−1.95	−3.32	−6.28
$0d_{\frac{3}{2}}$	−0.50	−0.50	−0.50	−0.50	−3.58
$1s_{\frac{1}{2}}$	−0.50	−0.50	−2.78	−3.66	−5.87

TABLE II. *HO* parameter values for *SP* wave functions and the associated r.m.s. charge radius for each nucleus. All experimental data were taken from Ref. [11].

	b (fm)	$<r^2>^{\frac{1}{2}}_{calc}$ (fm)	$<r^2>^{\frac{1}{2}}_{expt}$ (fm)
^{6}Li	1.650	2.40	2.55 ± 0.10
^{7}Li	1.650	2.36	2.41 ± 0.10
^{9}Be	1.630	2.40	2.50 ± 0.09
^{10}B	1.600	2.45	2.45 ± 0.12
^{12}C	1.600	2.44	2.4550 ± 0.0024
^{13}C	1.639	2.46	2.440 ± 0.025
^{16}O	1.701	2.58	2.730 ± 0.025
^{20}Ne	1.751	2.85	2.992 ± 0.008
^{27}Al	1.653	2.82	3.05 ± 0.05
^{28}Si	1.698	2.92	3.086 ± 0.018
^{40}Ca	1.905	3.38	3.482 ± 0.025
^{42}Ca	1.866	3.31	
^{44}Ca	1.880	3.33	
^{48}Ca	1.869	3.31	3.470
^{56}Fe	1.802	3.38	3.801 ± 0.015
^{58}Ni	1.923	3.64	3.764 ± 0.010
^{88}Sr	2.062	4.04	4.17 ± 0.02
^{90}Zr	2.041	4.02	4.258 ± 0.008
^{115}In	2.128	4.36	
^{120}Sn	2.174	4.46	4.640
^{197}Au	2.198	4.84	5.33 ± 0.05
^{208}Pb	2.326	5.15	5.521 ± 0.029

FIGURES

FIG. 1. The differential cross sections (top), the analysing powers (middle), and spin rotations (bottom) from the elastic scattering of 200 MeV protons from ^{6,7}Li. The data (dots) are compared with the results of our microscopic model calculation (solid curves). Data were taken from Ref. [23].

FIG. 2. As for Fig. 1 but for ^{9}Be and ^{10}B. Data were taken from Ref. [24].

FIG. 3. As for Fig. 1 but for ^{12,13}C. Data were taken from Ref. [25,26].

FIG. 4. As for Fig. 1 but for ^{16}O and ^{20}Ne. Data were taken from Ref. [26,27].

FIG. 5. As for Fig. 1 but for ^{27}Al and ^{28}Si. Data were taken from Ref. [29,30].

FIG. 6. As for Fig. 1 but for ^{40,42}Ca. Data were taken from Ref. [26,27,31].

FIG. 7. As for Fig. 1 but for ^{44,48}Ca. Data were taken from Ref. [26,31].

FIG. 8. As for Fig. 1 but for ^{56}Fe and ^{58}Ni. Data were taken from Ref. [29,32].

FIG. 9. As for Fig. 1 but for ^{88}Sr and ^{90}Zr. Data were taken from Ref. [33].

FIG. 10. As for Fig. 1 but for ^{115}In and ^{120}Sn. Data were taken from Ref. [29,34].

FIG. 11. As for Fig. 1 but for ^{197}Au and ^{208}Pb. Data were taken from Ref. [29,35].

FIG. 12. The variation of the oscillator lengths, b, scaled by $A^{-1/6}$ with mass.

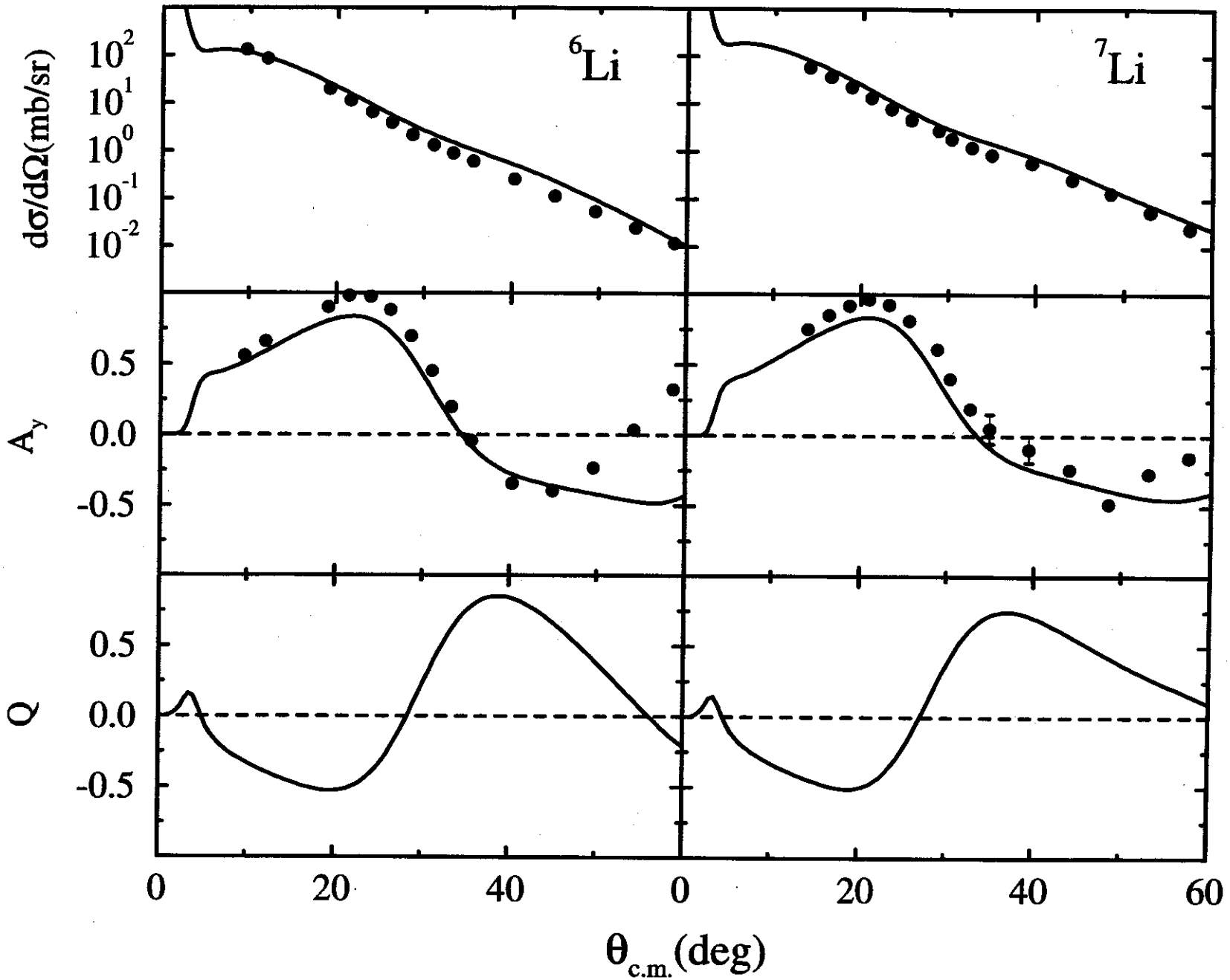
^{6}Li
^{7}Li
dσ/dΩ(mb/sr)
10^2
10^1
10^0
10^{-1}
10^{-2}
A_y
0.5
0.0
-0.5
Q
0.5
0.0
-0.5
0
20
40
0
20
40
60
$\theta_{c.m.}$(deg)

FIG. 4

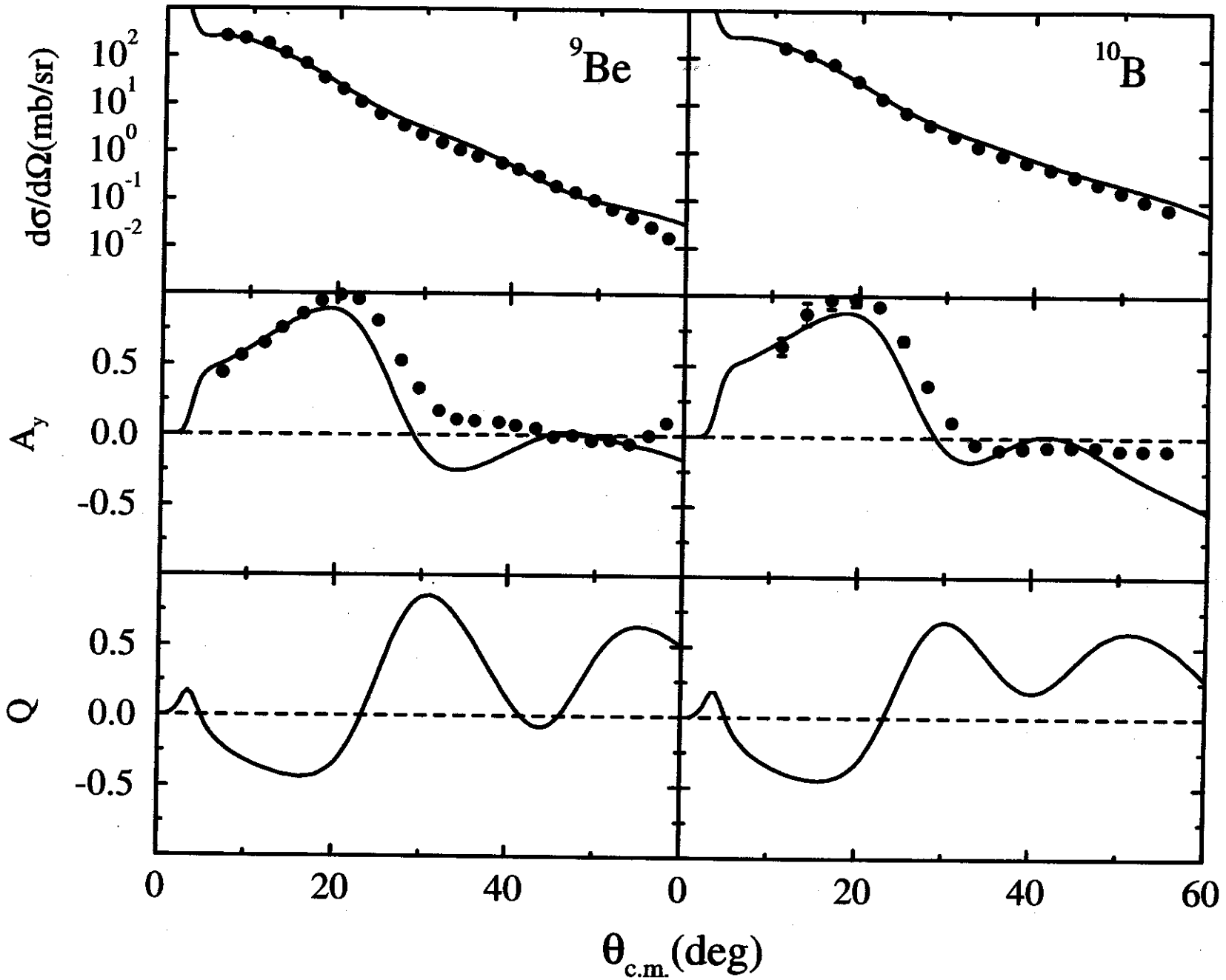
^{9}Be
^{10}B
dσ/dΩ(mb/sr)
10^{2}
10^{1}
10^{0}
10^{-1}
10^{-2}
A_y
0.5
0.0
-0.5
Q
0.5
0.0
-0.5
0
20
40
0
20
40
60
$\theta_{c.m.}$(deg)

Fig. 2

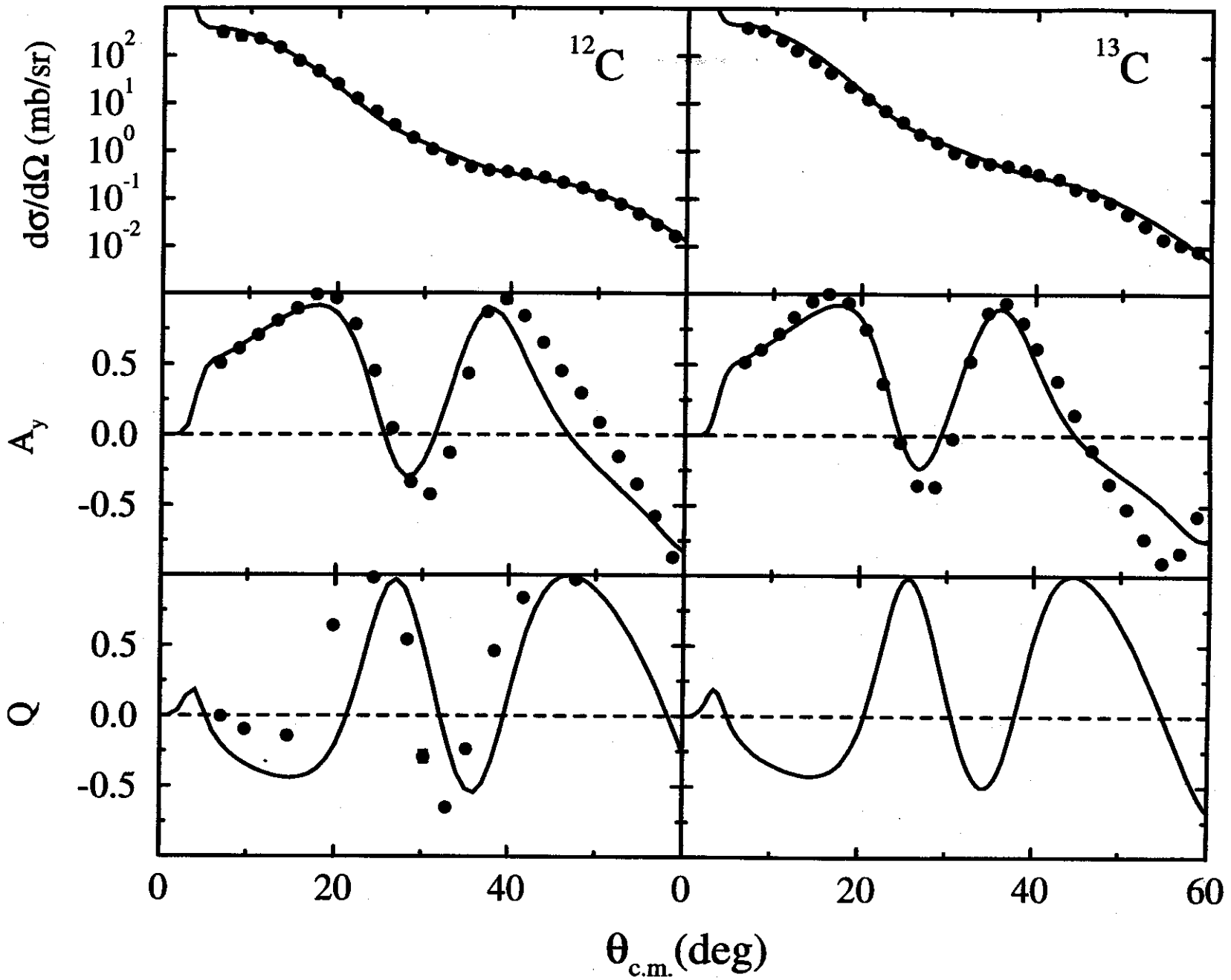
^{12}C
^{13}C
dσ/dΩ (mb/sr)
10^2
10^1
10^0
10^{-1}
10^{-2}
A_y
0.5
0.0
-0.5
Q
0.5
0.0
-0.5
0
20
40
0
20
40
60
$\theta_{c.m.}$(deg)

FIG. 3

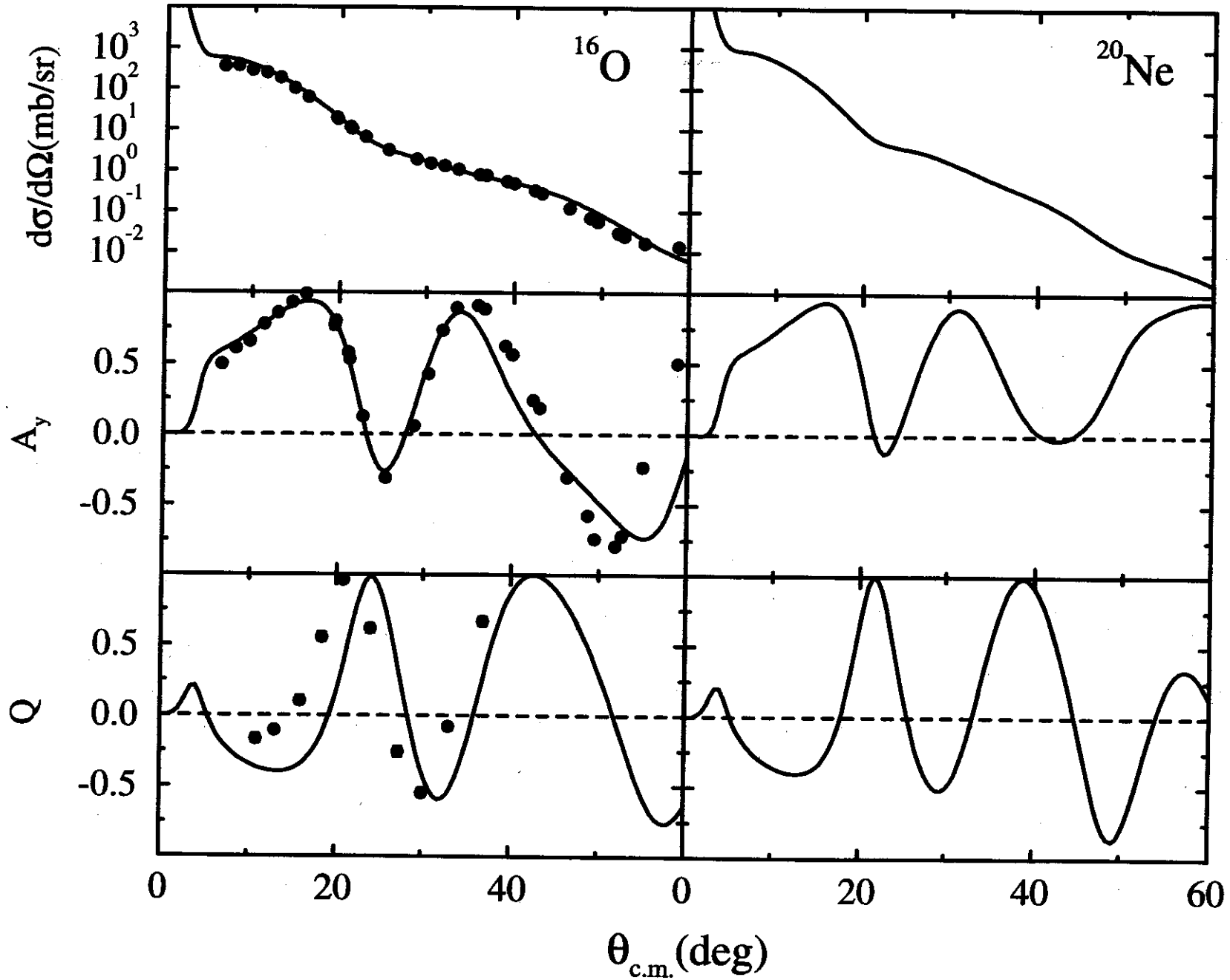
^{16}O
^{20}Ne
dσ/dΩ(mb/sr)
10^3
10^2
10^1
10^0
10^{-1}
10^{-2}
A_y
0.5
0.0
-0.5
Q
0.5
0.0
-0.5
0
20
40
0
20
40
60
$\theta_{c.m.}$(deg)

FIG. 4

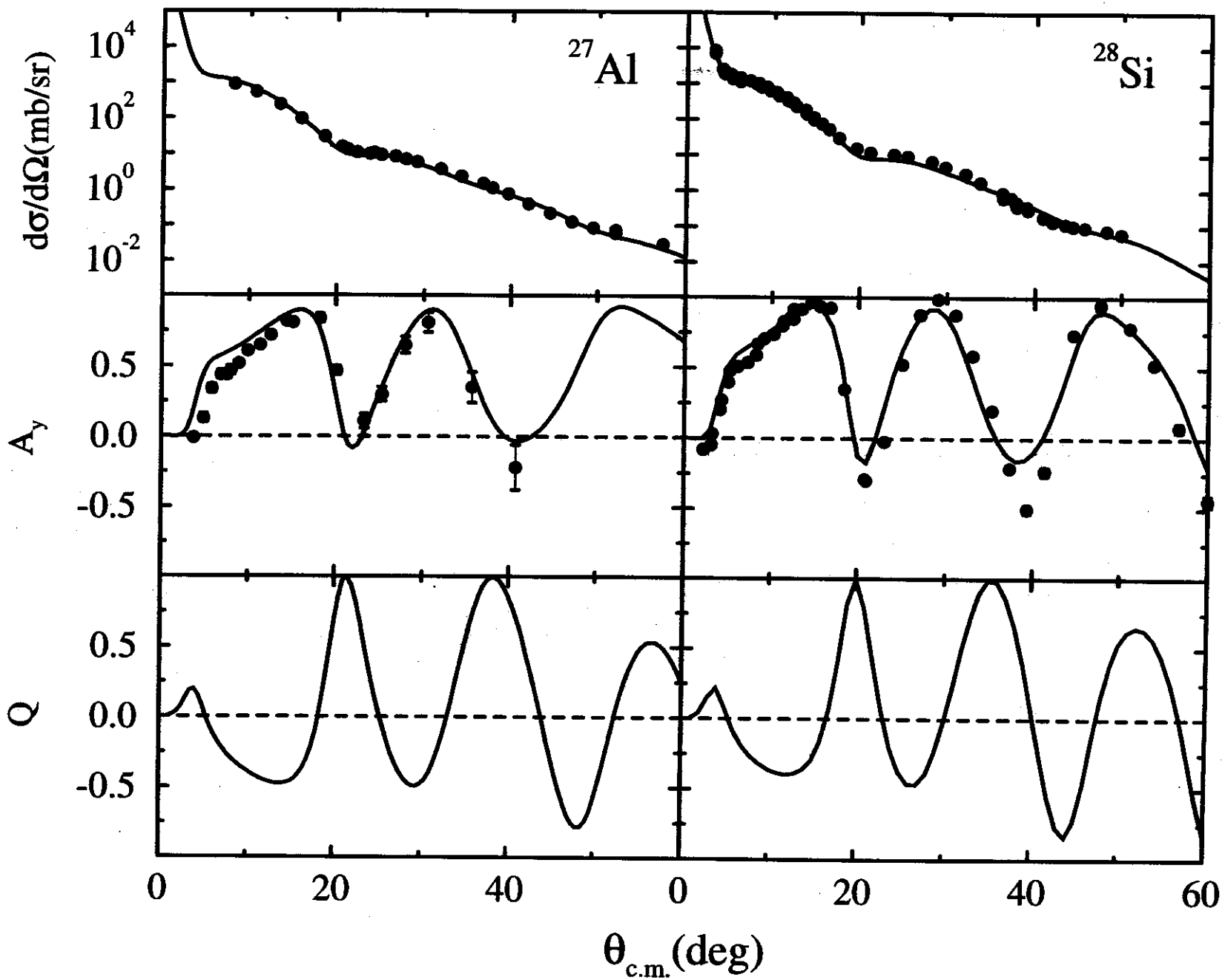
^{27}Al
^{28}Si
dσ/dΩ(mb/sr)
10^4
10^2
10^0
10^{-2}
A_y
0.5
0.0
-0.5
Q
0.5
0.0
-0.5
0
20
40
0
20
40
60
$\theta_{c.m.}$(deg)

Fig. 5

^{42}Ca
^{40}Ca
10^{4}
10^{2}
10^{0}
10^{-2}
dσ/dΩ (mb/sr)
0.5
0.0
-0.5
A_y
Q
0
20
40
60
$\theta_{c.m.}$ (deg)

FIG. 6

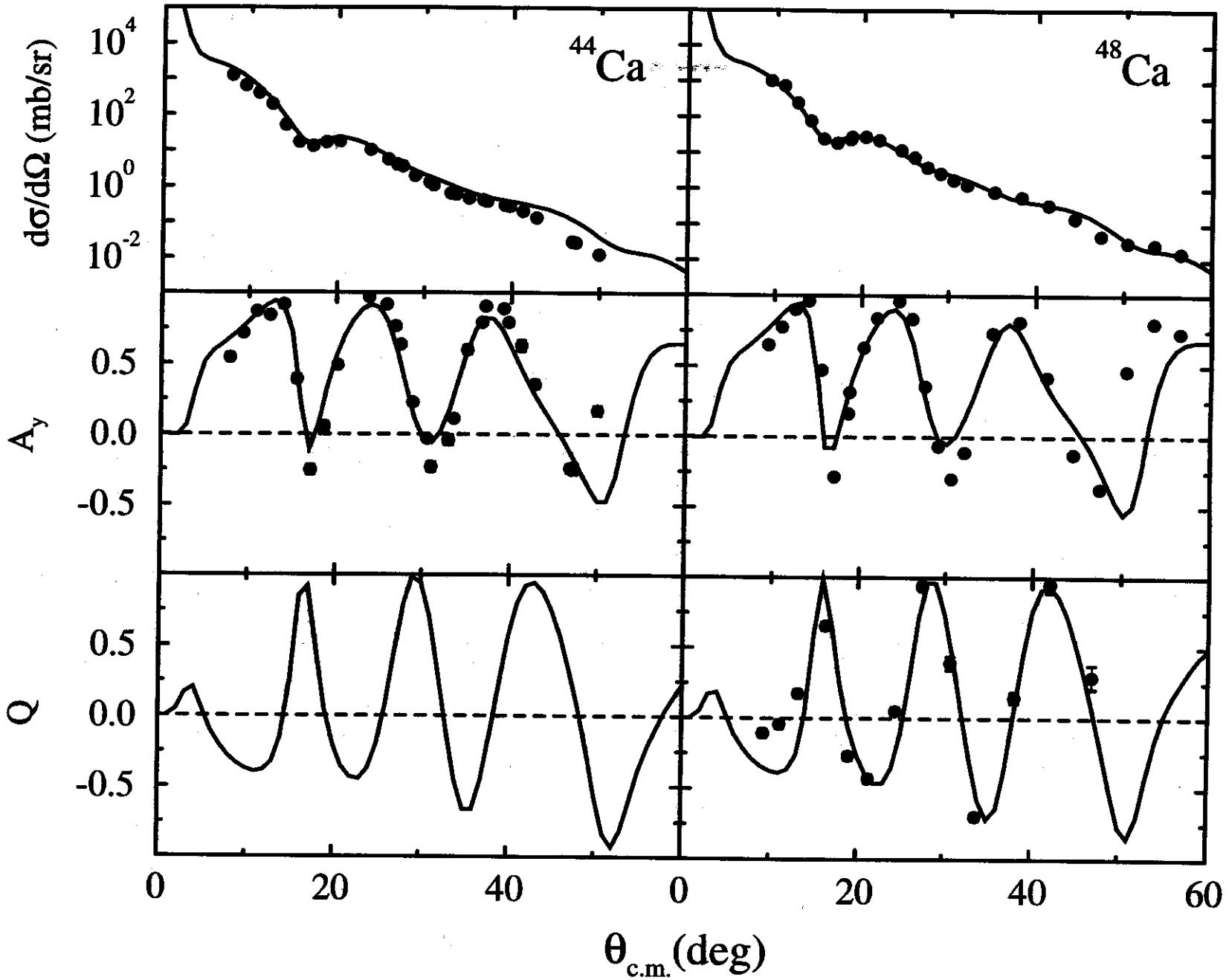
^{44}Ca
^{48}Ca
dσ/dΩ (mb/sr)
10^4
10^2
10^0
10^{-2}
A_y
0.5
0.0
-0.5
Q
0.5
0.0
-0.5
0
20
40
0
20
40
60
$\theta_{c.m.}$(deg)

Fig. 7

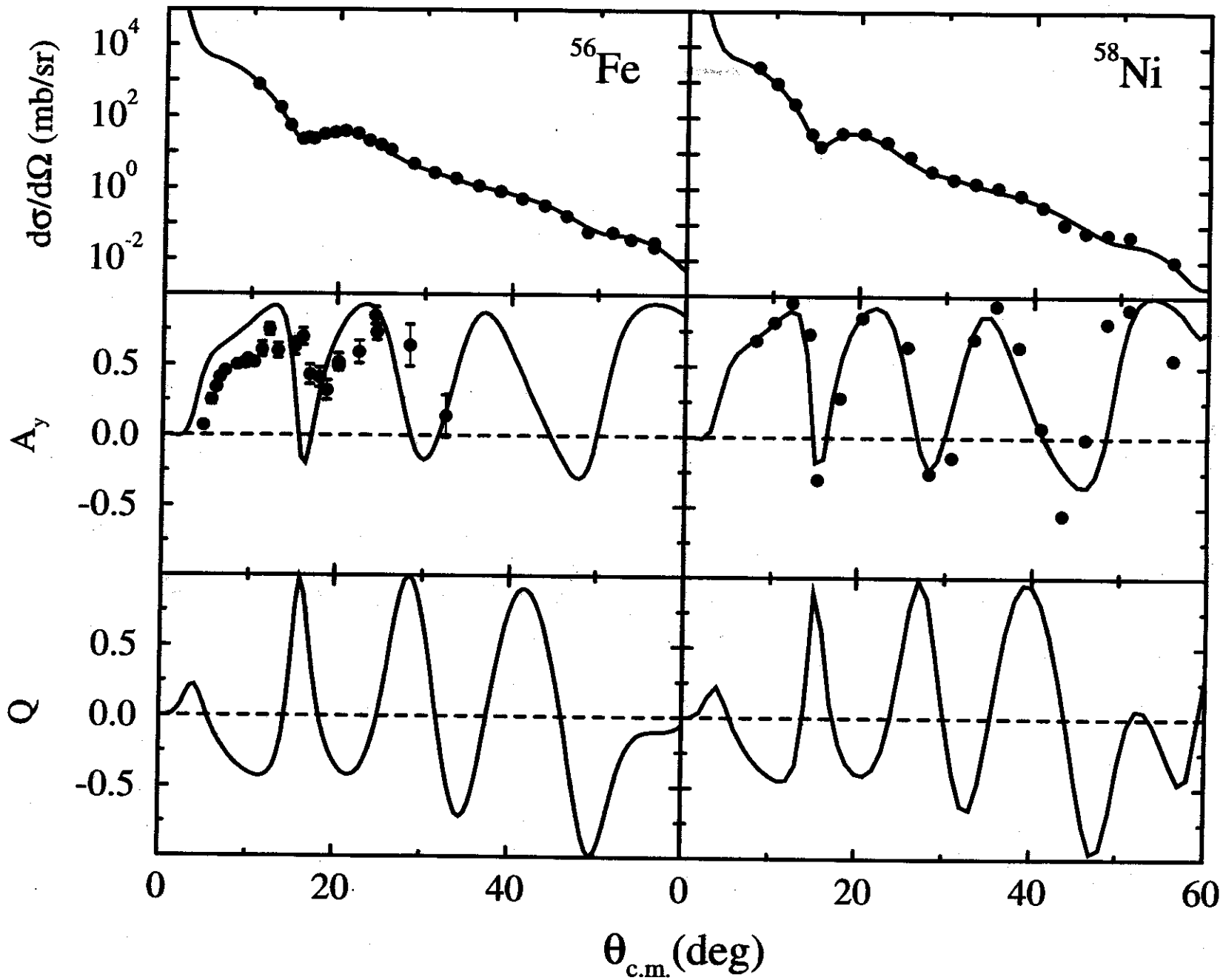
^{56}Fe
^{58}Ni
dσ/dΩ (mb/sr)
10^4
10^2
10^0
10^{-2}
A_y
0.5
0.0
-0.5
Q
0.5
0.0
-0.5
0
20
40
0
20
40
60
$\theta_{c.m.}$(deg)

Fig. 8

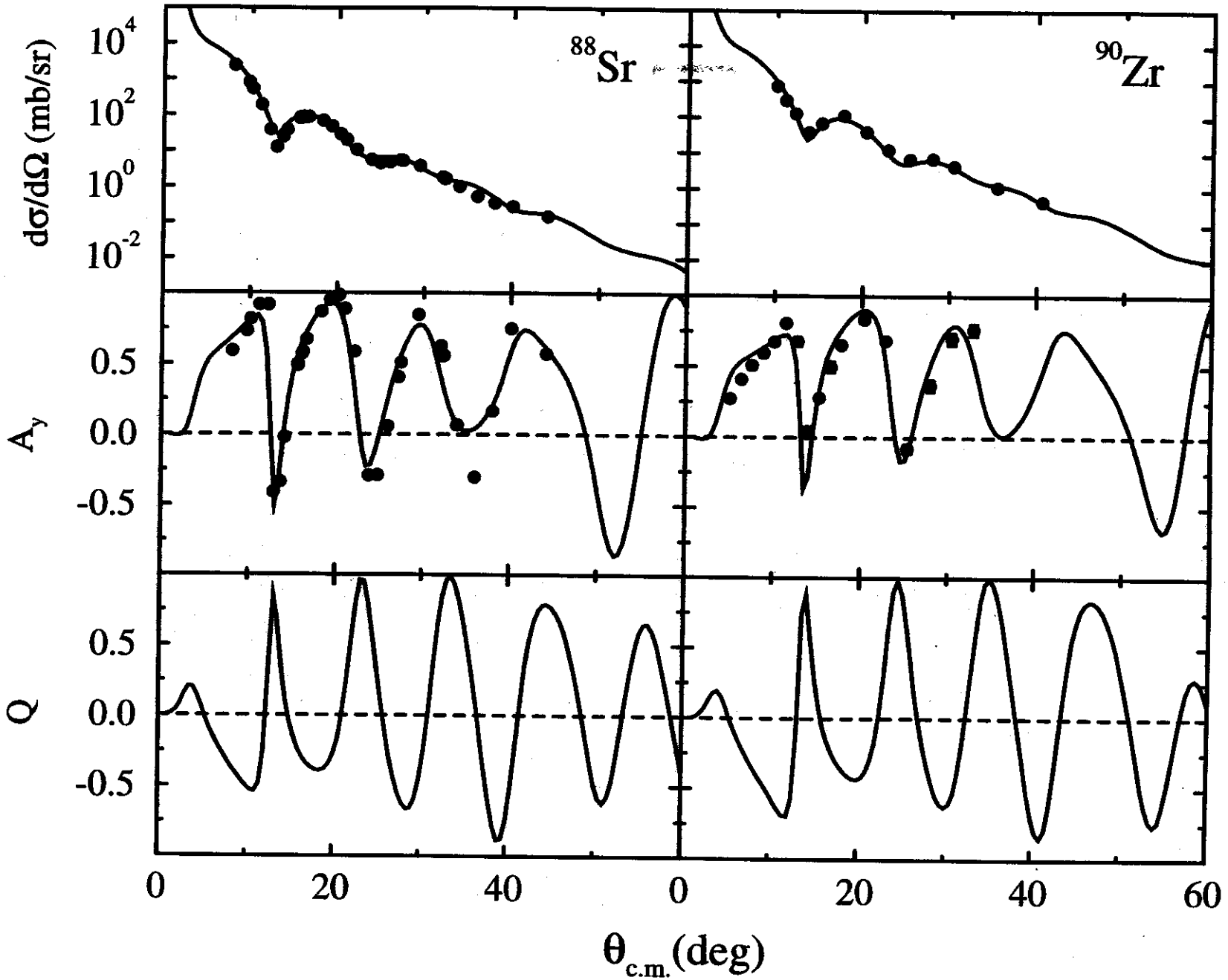
^{88}Sr
^{90}Zr
dσ/dΩ (mb/sr)
10^4
10^2
10^0
10^{-2}
A_y
0.5
0.0
-0.5
Q
0.5
0.0
-0.5
0
20
40
0
20
40
60
$\theta_{c.m.}$(deg)

FIG. 9

^{120}Sn
^{115}In
dσ/dΩ (mb/sr)
10^4
10^2
10^0
10^{-2}
A_y
0.5
0.0
-0.5
Q
0.5
0.0
-0.5
0
20
40
0
20
40
60
$\theta_{c.m.}$ (deg)

FIG. 10

^{208}Pb
^{197}Au
dσ/dΩ (mb/sr)
10^4
10^2
10^0
10^{-2}
A_y
0.5
0.0
-0.5
Q
0.5
0.0
-0.5
0
20
40
0
20
40
60
$\theta_{c.m.}$ (deg)

FIG. 11

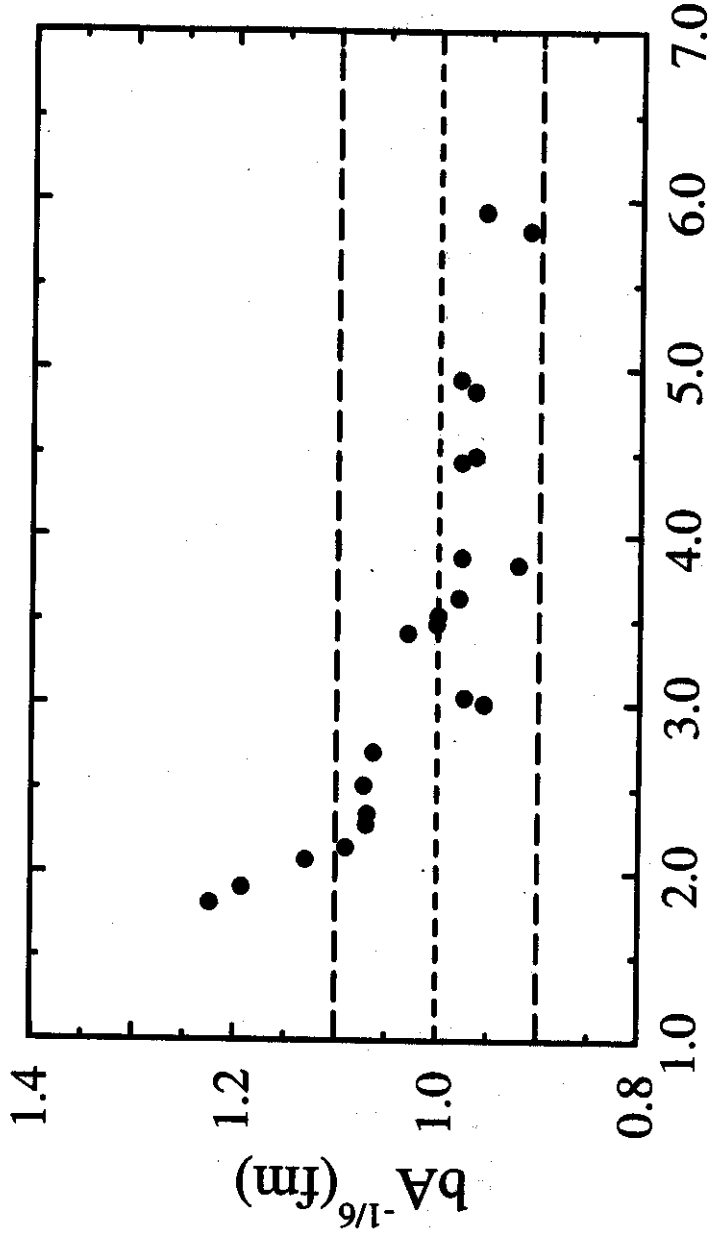

FIG. 12